Carbon sources and sinks from an Ensemble Kalman Filter ocean data assimilation

M. Gerber

Climate and Environmental Physics, Physics Institute, University of Bern, 3012 Bern, Switzerland.

F. Joos

Climate and Environmental Physics, Physics Institute, University of Bern, 3012 Bern, Switzerland and Oeschger Centre for Climate Change Research, University of Bern.

M.Gerber, Climate and Environmental Physics, Physics Institute, University of Bern, 3012 Bern, Switzerland. (mgerber@climate.unibe.ch)

Abstract. We quantify contemporary and preindustrial net air-sea CO_2 fluxes by an Ensemble Kalman Filter assimilation of interior ocean observations and compare results with published estimates in the light of data and model uncertainties. Four different published reconstructions of anthropogenic carbon and the ΔC_{gasex} tracer are assimilated into different versions of the Bern3D ocean model. The two tracers represent the components of dissolved inorganic carbon due to the anthropogenic perturbation and due to the air-sea gas exchange of natural CO_2. Contemporary air-sea fluxes for broad latitudinal bands are consistent with those from earlier ocean inversions and the observed air-sea CO_2 partial pressure differences. Best agreement with the pCO_2-based contemporary fluxes is found for the TTD anthropogenic carbon reconstruction. We infer modest meridional transport rates of up to 0.5 GtC yr^{-1} for the preindustrial and the contemporary ocean and a small carbon transport across the equator. The anthropogenic perturbation offsets the preindustrial net sea-to-air flux yielding a weak contemporary carbon sink in the Southern Ocean (south of 44^oS) of 0.15 ± 0.25 GtC yr^{-1}. Preindustrial Southern Ocean outgassing varies by almost a factor of two among the four ΔC_{gasex} reconstructions. Large differences in regional fluxes are found between an earlier ocean inversion using Green's function and this study for the same model and input data calculation. Systematic differences in assimilated and optimized ΔC_{gasex} fields are large in both inversions and the contemporary, anthropogenic, and preindustrial air-sea CO_2 flux in the high and mid-latitude Southern Hemisphere remain uncertain.

1. Introduction

Human activities cause atmospheric carbon dioxide (CO_2) and its radiative forcing to rise at at speed that is unprecedented for at least the last 20,000 years and well above the natural range of at least the past 800,000 years [*Lüthi et al.*, 2008; *Joos and Spahni*, 2008]. The main cause for the perturbation in CO_2 and climate are carbon emissions from fossil fuel use and land use changes. A quantitative understanding of the marine sources and sinks of CO_2 is an important element for understanding the role of the carbon cycle and climate-carbon cycle interactions in global warming projections [*Denman et al.*, 2007]. The contemporary air-sea fluxes of CO_2 are conceptually often separated into "natural" and "anthropogenic" components to discuss and quantify physical and biogeochemical mechanisms driving carbon sources and sink fluxes and changes in carbon inventories. The natural part represents the air-sea flux before the beginning of the industrialization (~1750 AD), when the carbon cycle was relatively close to equilibrium on decadal to centennial time scales. The anthropogenic component is the perturbation from the preindustrial state.

It has remained challenging to accurately quantify carbon sources and sink fluxes and underlying mechanisms, in part because of the large spatio-temporal variability of CO_2 fluxes [e.g. *Bakker et al.*, 2001], in part because it is not possible to measure the natural and anthropogenic components of the CO_2 air-sea flux, and of the carbon fluxes and stocks within the ocean separately.

Major scientific efforts have been dedicated to quantify natural and anthropogenic and contemporary carbon fluxes and stocks using both data and models. A set of studies aims to separate the natural and anthropogenic component of the inorganic carbon in the ocean from tracer data and to reconstruct the detailed spatial distribution of natural and anthropogenic carbon (C_{anth}) in the ocean [e.g. *Chen and Millero*, 1979; *Heimann and Maier-Reimer*, 1996; *Gruber et al.*, 1996; *Sabine et al.*, 2004; *Álvarez et al.*, 2009; *Vázquez Rodríguez et al.*, 2009]. Reconstructions yield consistently large C_{anth} inventories in the North Atlantic and in the southern mid-latitude ocean, but considerable discrepancies in Southern Ocean inventories are found between different observation-based methods [*Álvarez et al.*, 2009; *Vázquez Rodríguez et al.*, 2009].

Another string of work is directed to establish the spatio-temporal distribution of the air-sea difference in the partial pressure of CO_2 (pCO_2) to calculate, in combination with an air-sea transfer velocity [e.g. *Wanninkhof*, 1992; *Müller et al.*, 2008], carbon fluxes [*Tans et al.*, 1990; *Takahashi et al*, 2008].

Alternatively, inverse approaches are utilized to infer inter alia contemporary air-sea fluxes of carbon from atmospheric and oceanic data in combination with transport models [e.g. *Enting and Mansbridge*, 1989; *Gloor et al.*, 2003; *Baker et al*, 2006; *Jacobson et al.*, 2007; *C. Rödenbeck et al.*, 2008]. Inversions of the observed atmospheric CO_2 gradient yield agreement in flux for large latitudinal bands [*Denman et al.*, 2007], but reveal a large sensitivity of inferred regional fluxes to model details and suffer from the sparse CO_2 sampling network with 60-120 stations [*Kaminski et al.*, 2001]. In contrast, the oceanic carbon distribution has been established by thousands of measurements [*Key et al.*, 2004]. Recently, the natural and anthropogenic air-sea fluxes of CO_2 have been quantified from data-based reconstructions of C_{anth} and the tracer ΔC_{gasex} [*Gloor et al.*, 2003; *Mikaloff Fletcher et al.*, 2006, 2007; *Gerber et al.*, 2008]. The ΔC_{gasex} tracer reflects the component of the total inorganic carbon which is due to the natural air-sea exchange of CO_2 (see section 2.1). *Gruber et al.* [2009], summarizing results from *Mikaloff Fletcher et al.* [2006, 2007], found in general consistency between the contemporary air-sea fluxes from the ocean inversion and the fluxes derived from the surface ocean partial pressure field of CO_2 [*Takahashi et al*, 2008] and atmospheric inversions [*Baker et al*, 2006]. Uncertainties from input data or ocean transport have been quantified [*Mikaloff Fletcher et al.*, 2006, 2007; *Gerber et al.*, 2008]. *Mikaloff Fletcher et al.* [2006, 2007] use the Green's function of ten different ocean model or model setups to quantify uncertainties related to ocean transport. An area of concern is that the assimilated data are not directly observed, but computed from oceanic tracer distributions using constant stochiometric ratios. *Mikaloff Fletcher et al.* [2007] found that depth-dependent ratios strongly affect air-sea fluxes in regions that ventilate the deep ocean, most notably the Southern Ocean. *Gerber et al.* [2008] assessed uncertainties from systematic biases in the reconstructions of anthropogenic carbon (C_{anth}) by assimilating four global and six Atlantic reconstructions in their Ensemble Kalman Filter approach. The results indicate that the uptake and partitioning of carbon fluxes in the Southern Ocean remain uncertain and the explicit consideration of uncertainties in the C_{anth} reconstructions yields larger error bars for the inferred fluxes than derived by [*Mikaloff Fletcher et al.*, 2006] and discussed by [*Gruber et al.*, 2009]. A disturbing feature of the inversion for preindustrial air-sea fluxes is the presence of substantial residuals in the ΔC_{gasex} tracer [*Mikaloff Fletcher et al.*, 2007; *Gruber et al.*, 2009] pointing to unsolved problems and rising a number of questions. How robust are inverse estimates for the Southern Ocean region where large discrepancies in reconstructed anthropogenic carbon are found? How do uncertainties in published data-based estimates of C_{anth} impact on the reconstruction of ΔC_{gasex} and preindustrial carbon fluxes? Are the results of ocean inversion studies as sensitive to the details of the experimental setup and methods as those from atmospheric inversions?

The aim of this study to quantify preindustrial and contemporary air-sea and meridional ocean carbon fluxes on the regional scale and to explore their uncertainties. We complement our earlier inversion of C_{anth} data [*Gerber et al.*, 2008]) by assimilating ΔC_{gasex} data in the Bern3D model [*Müller et al.*, 2006] using an Ensemble Kalman Filter method (EnKF) [*Evensen*, 2003]. There are a number of new elements compared to earlier studies. Four different published reconstructions of C_{anth} are utilized to compute ΔC_{gasex}. These reconstruction methods are: The ΔC^* method [*Gruber et al.*, 1996], the TTD method [*Waugh et al.*, 2006], the CFC-shortcut method [*Thomas and Ittekkot*, 2001] and the TrOCA method [*Touratier and Goyet*, 2004; *Touratier et al.*, 2007]. The data are assimilated into different dynamical setups of the Bern3D ocean model. The ΔC_{gasex} is usually normalized to have on average a surface concentration of zero. Here, we explore the impact on results of an alternative normalization. The influence of a potential bias or mismatch in the seasonality of the air-sea CO_2 flux and ocean transport is investigated. Last but not least, the application of an EnKF provides an alternative to the Green's function approach applied by *Mikaloff Fletcher et al.* [2006, 2007] or to other data assimilation methods [*Schlitzer*, 2002, 2007].

2. Method

2.1. Data

We use a quasi-conservative tracer, ΔC_{gasex} [*Sarmiento and Gruber*, 2006] to infer preindustrial air-sea CO_2 fluxes. The underlying hypothesis is that gradients in ΔC_{gasex}

are only driven by air-sea CO_2 fluxes and by physical (advection, convection, diffusion) transport within the ocean. ΔC_{gasex} is computed from measured total inorganic carbon (C_T) by removing the reconstructed anthropogenic component C_{ant}, and the estimated signals from the remineralization of organic material and calcium carbonate by assuming constant stochiometric ratios between carbon and phosphate, $r_{C:P}$, and between phosphate (PO_4^{3-}) and nitrate, $r_{N:P}$ in the remineralization flux of organic matter and a ratio of 0.5 between carbon and alkalinity (Alk) in calcium carbonate:

$$\Delta C_{gasex} = \frac{S_0}{S}(C_T - r_{C:P}PO_4^{3-} - 0.5(Alk + r_{N:P}PO_4^{3-})) - C_{anth} - const. \qquad (1)$$

ΔC_{gasex} is computed for all available section-data points of the GLODAP database [*Key et al.*, 2004] (http://cdiac.esd.ornl.gov/oceans/glodap/GlopDV.htm) and the values assigned to the appropriate grid cell of the Bern3D model. $r_{C:P}$ and $r_{N:P}$ are set to 117 and 16 [*Anderson and Sarmiento*, 1994]. The constant *const* is chosen to yield a mean surface concentration, or alternatively global ocean inventory, of zero. ΔC_{gasex} is normalized to a reference salinity $S_0 = 35 psu$. The anthropogenic perturbation is removed using four observation-based reconstructions of C_{anth}. The C_{anth} estimates from the ΔC^*, TTD and CFC-shortcut reconstructions are available from the GLODAP site. The TrOCA C_{anth} estimates are calculated following *Touratier et al.* [2007] from the GLODAP section data. A detailed comparison of different C_{anth} data can be found in *Vázquez Rodríguez et al.* [2009], a short overview of the methods is presented in *Gerber et al.* [2008], and further details are available from the original publications [*Gruber et al.*, 1996; *Thomas and Ittekkot*, 2001; *Waugh et al.*, 2004; *Touratier et al.*, 2007]. Three of the reconstruction methods (ΔC^*, TTD and CFC-shortcut) have been investigated in the framework of an OGCM [*Matsumoto and Gruber*, 2005; *Waugh et al.*, 2006; *Matear et al.*, 2003]. The ΔC^*

method shows a tendency towards overestimation of C_{anth} in young water masses, but underestimation in old water [*Matsumoto and Gruber*, 2005]. The TTD method tends to be biased high in the Southern Ocean due to the assumed temporally constant air-sea CO_2 disequilibrium [*Waugh et al.*, 2006]. The CFC-shortcut method is not very reliable for old waters masses such as those in the deep ocean and those found in the Southern Ocean [*Matear et al.*, 2003; *Waugh et al.*, 2006]. Two recent studies comparing different C_{anth} reconstructions in the Atlantic and the Indian suggest that the ΔC^* method yields too low C_{anth} inventories in the Southern Ocean [*Vázquez Rodríguez et al.*, 2009; *Álvarez et al.*, 2009]

2.2. Model Setup

2.2.1. Optimization scheme

The approach of *Gerber et al.* [2008] is used with a few adaptation and a brief overview is given next. Further detail are found elsewhere [*Gerber et al.*, 2008; *Evensen*, 2003, 2004]. The global ocean surface of the Bern3D model is divided into 17 regions (Figure S1) for which the natural net air-sea flux of carbon is optimized. The air-sea flux of CO_2 for each model region F_l is described as the product of a spatio-temporal pattern, $P(i,j,t)$, and a scaling parameter, ψ:

$$F_l(i,j,t) = P(i,j,t)\psi(l) \tag{2}$$

P is scaled to a unit flux (integrated over the region and year). ψ is the magnitude of the air-sea flux as optimized in the EnKF analysis scheme for each region l. The seasonal pattern $P(i,j,t)$ is based on the CO_2 air-sea flux climatology of *Takahashi et al.* [2002]. The air-sea fluxes of carbon act as a source or sink of ΔC_{gasex} in the Bern3D model. ΔC_{gasex} is transported as a conservative tracer within the model ocean. After spin up of the circulation, the Bern3D is initialized with a ΔC_{gasex} concentration of zero and integrated over 3000 years. In the EnKF, an ensemble of 32 members is applied and each member is forced with a set of the 17 flux scaling parameters ψ_l. The ensemble members are optimized in a way that minimizes the deviation between data-based estimates and modeled distribution of the ΔC_{gasex} tracer. The optimization is repeated until convergence of the solution, typically reached after a few iteration steps. The initial scaling parameters for any region are normally distributed around zero. The ensemble size has been tested in a simulation, where we included 64 instead of 32 ensemble members. Deviations in the inferred air-sea fluxes are less than 0.05 GtC yr^{-1}, except for the Southern Ocean, where we find a deviation up to 0.08 GtC yr^{-1}. The root-mean-square-error (RMSE) between optimized and observation-based ΔC_{gasex} remains the same.

2.2.2. Bern3D Model configurations

The Bern3D ocean model [*Müller et al.*, 2006] is a cost-efficient coarse resolution global circulation model based on the ocean model of [*Edwards and Marsh*, 2005]. Model results are found to be in good agreement with observed distribution of different tracers [*Müller et al.*, 2006, 2008; *Parekh et al.*, 2008; *Tschumi et al.*, 2008]. As in *Gerber et al.* [2008], four different model setups with different circulation patterns or mixing are used to assess uncertainties associated with ocean transport. These have been built to investigate existing shortcomings in the circulation of the Bern3D model. The four model configurations include the (i) *Standard* setup as described in *Müller et al.* [2006]; (ii) the *ACC* $\times$ *3* , which includes a strengthening of the Antarctic Circumpolar Current (ACC) by a factor of three and a salt flux from the Pacific to the North Atlantic. Increasing the strength of the ACC results in a northward expansion of the ACC and lowers the strength of the southern subtropical gyres. The inserted salt flux increases the formation and propagation of the North Atlantic Deep Water (NADW); (iii) the *PSI × 3* setup, which is the standard setup modified by increasing the barotropic streamfunction globally by a factor of three and applying the same salt flux as in the ACC × 3 setup. The increased barotropic streamfunction leads to strong horizontal and vertical mixing of tracers in all basins. (iv) the *High Diffusion* setup is the same as the standard setup except that diapycnal diffusion is increased by a factor of four for passive tracer and is set to 4×10^{-5} m s^{-2}. Figure (S2) shows the overturning of the different circulation setups. The Green's function of the standard setup has been used earlier in the inversions of *Mikaloff Fletcher et al.* [2006, 2007]. The skill of the Bern3D model in representing the observation-based radiocarbon distribution compares with a score of 0.93 favorably to that of general circulation ocean models with a range of skill scores from 0.65 to 0.94 [*Mikaloff Fletcher et al.*, 2007].

2.3. Calculation of contemporary air-sea fluxes and of best estimates

Contemporary air-sea fluxes for each region are calculated as the sum of the natural fluxes inferred from the ΔC_{gasex} tracer, the anthropogenic air-sea fluxes of *Gerber et al.* [2008] for the nominal year 1995, and a river-derived outgassing taken from *Jacobson et al.* [2007] and as used in *Gruber et al.* [2009]. The input of organic and inorganic carbon by rivers causes an outgassing of CO_2 [*Sarmiento and Sundquist*, 1992] that is not resolved by the inversion.

Best estimates are calculated by averaging the results obtained for the four different ΔC_{gasex} fields. Individual estimates are weighted using the same skill score as *Gerber et al.* [2008] and derived from the assimilated and modeled C_{anth} fields. For ocean transport and river outgassing, we apply the same uncertainties as *Gruber et al.* [2009]. Overall uncertainties are estimated by adding uncertainties from the ΔC_{gasex} fields, ocean transport, and river-driven outgassing using Gaussian error propagation. All uncertainties provided represent $\pm$ 1 standard deviation.

3. Results

3.1. Large-scale carbon sources and sink fluxes

.

The results of the Ensemble Kalman Filter (EnKF) inversion are aggregated for each basin into broad latitudinal bands to ease comparison with other studies. The aggregated Bern3D-EnKF inversion yields the familiar pattern of outgassing of CO_2 in the tropics and ocean uptake in the temperate and high latitude ocean (Figure 1). The contemporary (1995 AD) tropical source (19^{o}S to 16^{o}N) is estimated to be 0.60 $\pm$ 0.16 GtC yr^{-1}. The contemporary high-latitude sinks are 0.15 $\pm$ 0.25 GtC yr^{-1} in the Southern Ocean and 0.25 $\pm$ 0.07 GtC yr^{-1} in the northern North Atlantic. The sink in the mid latitude ocean amounts to 1.20 $\pm$ 0.16 GtC yr^{-1} in Southern and to 0.64 $\pm$ 0.13 GtC yr^{-1} in the Northern Hemisphere.

The attribution of the contemporary fluxes to a preindustrial flux (natural plus riverine outgassing), and to an anthropogenic perturbation reveals underlying oceanographic mechanisms (Table 1 and Figure 2). The perturbation flux is into the ocean in all regions, with largest sink fluxes of C_{anth} into the Southern Ocean. At preindustrial time, the inferred tropical source is larger than today, whereas the temperate and northern high-latitude sink fluxes are considerably smaller than today. In the Southern Ocean, the natural (preindustrial) component corresponds to a source of 0.69 ± 0.15 GtC yr^{-1} that is more than offset by an uptake flux of 0.86 ± 0.25 GtC yr^{-1} of C_{anth}.

The flux patterns are consistent with the generally accepted picture of ocean circulation and the observed surface temperature and nutrient distributions. The preindustrial pattern is the result of the interplay of the solubility pump and the biological pump [*Volk and Hoffert*, 1985; *Maier-Reimer*, 1993; *Murnane et al.*, 1999; *Sarmiento et al.*, 2000]. Warming causes the pCO_2 to rise favoring outgassing in the warm tropical region and uptake in the mid- and high-latitude ocean. Formation of organic material tends to lower pCO_2, whereas remineralization tends to enhance pCO_2. Consequently, we expect a tendency towards CO_2 outgassing in regions where nutrient and carbon rich water is brought to the surface and uptake from the atmosphere where organic matter is formed. Thus, the CO_2 outgassing in the tropics and in the Southern Ocean is explained by upwelling of nutrient rich waters, whereas the sink in mid-latitude regions and in the high latitude North Atlantic is consistent with the low nutrient concentrations and with cooling of poleward flowing waters.

In the inversion, the preindustrial air-sea flux is a direct consequence of the gradients in ΔC_{gasex} and ocean model transport. For example, Circumpolar Deep Water (CPDW) with high ΔC_{gasex} concentrations is transported towards the surface, moving northward by the Ekman drift and subsequently transformed into Antarctic Intermediate Water (AAIW). Thus, the decrease in ΔC_{gasex} concentration of order 50 μmol between CPDW to AAIW implies a strong CO_2 outgassing in the Southern Ocean.

Turning to the anthropogenic perturbation, the accelerating atmospheric CO_2 growth, causes a positive perturbation in the surface atmosphere-ocean partial pressure difference relative to the natural, preindustrial situation and uptake of C_{anth} in all regions. The uptake of C_{anth} is expected to be particularly large in regions were "old" water, that has a low concentration of C_{anth} and a large potential for C_{anth} uptake, is upwelled or mixed by convection into the surface. A confounding factor is warming and cooling. Warming has the tendency to enhance C_{anth} uptake as the Revelle factor and thus the uptake capacity for C_{anth} is lower for warm than for cold water. The strong anthropogenic uptake flux in the Southern Ocean appears to be driven by upwelling of Circumpolar Deep Water and subsequent warming as the water is moved northwards by the Ekman drift before being subducted as AAIW and Subantarctic Mode Water (SAMW). This results in large C_{anth} inventories in the Southern Hemisphere mid-latitude ocean [*Sabine et al.*, 2004]. Uptake fluxes per unit area are also relatively high in the upwelling regions of the tropics and in the Nordic Seas where convection and North Atlantic Deep Water formation carry C_{anth} efficiently to the abyss. (Figure S2).

The reconstructed contemporary fluxes for broad latitudinal bands of individual ocean basins are broadly consistent with the results of the Green's function ocean inversion (GFOI) [*Gruber et al.*, 2009], the fluxes from the pCO_2 climatology [*Takahashi et al*, 2008], and the atmospheric inversion of *Baker et al* [2006]. The EnKF results agree with the results from the GFOI for each aggregated region within their uncertainties. Differences between the two studies are large for the Southern Ocean and the Pacific Mid Latitude region. The EnKF inversion, as well as the GFOI, yield higher contemporary uptake fluxes in the southern mid-latitudes than the pCO_2 climatology. The disagreement is particularly striking for the temperate Pacific region, a region where sampling density for the pCO_2 climatology is low [*Takahashi et al*, 2008]. Interestingly, the atmospheric inversion of *Baker et al* [2006] suggests a small net sea-to-air flux in the mid-latitude Southern Pacific, a finding that is in strong contrast to the uptake flux inferred by all oceanographic methods.

Next, we follow the setup of *Gerber et al.* [2008] for anthropogenic fluxes and investigate uncertainties in natural fluxes by applying different ocean transport fields and different reconstructions of ΔC_{gasex}. In addition, we explore sensitivity of air-sea fluxes to the prescribed seasonal flux pattern.

3.2. Uncertainties in inferred natural air-sea CO_2 fluxes

3.2.1. Sensitivity of natural air-sea fluxes to ocean transport and to prescribed seasonal flux pattern

Four different circulation setups of the Bern3D ocean model are applied with the same ΔC_{gasex} data. The latter are computed by removing the anthropogenic signal reconstructed with the ΔC^* method [*Gruber et al.*, 1996; *Key et al.*, 2004] and by normalizing the ΔC_{gasex} field to have zero average surface concentration. A few regions are particularly sensitive to changes in circulation: the polar and subpolar Southern Ocean, the high-latitude North Atlantic, and the southern mid-latitude regions (Table 2).

The more vigorous Atlantic overturning and the deeper penetration of NADW in the

"ACC" and "PSI × 3" setups leads to a higher uptake flux in the high- and mid-latitude North Atlantic. The inferred uptake flux north of 34^oN in the Atlantic is more than twice as high for these two settings than for the standard setup. Consequently, the export of ΔC^* from the deep North Atlantic to the Southern Hemisphere is enhanced. The enhanced strength of the circumpolar currents causes a more vigorous exchange between the Southern Ocean and the mid-latitude ocean, enhancing uptake in the mid-latitude Pacific and mid-latitude Indian regions and outgassing in the Southern Ocean. The increased uptake in the North Atlantic and the Pacific and Indian southern mid-latitude regions is mostly balanced by enhanced outgassing in the Southern Ocean region by 0.19 and 0.30 GtC yr^{-1}, and a decrease in the aggregated net air-to-sea flux in the mid-latitude and tropical Atlantic (46^oS to 34^oN) by 0.14 and 0.18 GtC yr^{-1} relative to the standard setup. Increasing vertical diffusivity for passive tracers by a factor of four has a small effect ($<$ 0.06 GtC yr^{-1})on inferred sources and sinks (Table 2).

Observation-based concentrations of ΔC_{gasex} are much higher than model results in the deep Pacific and Atlantic (Figure 3). We have modified the seasonal pattern for the northern high latitude Atlantic and for the polar Southern Ocean towards larger uptake rates during the winter time and less uptake or even outgassing during summer time. Thereby, we tend to increase the ΔC_{gasex} concentrations in the surface during times of deep water formation in the Nordic Seas and the Southern Ocean and to reduce the data-model difference in the deep. Technically, the seasonal pattern of the two regions has been shifted by an offset of $0.95 \times \bar{p_n}$ where $\bar{p_n}$ is the temporal and spatial average flux of each grid box:

$$\tilde{p}(i,j,t)_n = \frac{p(i,j,t)_n - 0.95\bar{p}}{\int_{i,j,t}(p(i,j,t) - 0.95\bar{p})} \quad (3)$$

We emphasize that there is no reason to modify the prescribed spatio-temporal pattern from the pCO_2 climatology in such a drastic way and that this modification represents an extreme case. The inferred uptake pattern in the North Atlantic is changing towards less uptake in the North Atlantic High Latitude region, entirely compensated by increased uptake in the Northern Mid Latitude region. The Southern Ocean outgassing is reduced by 0.07 GtC yr^{-1} relative to the standard and uptake in the Atlantic Southern Mid-latitude region is reduced from 0.23 to 0.09 GtC yr^{-1}, whereas results are similar as in the standard setup for other regions. The modification in seasonal forcing did not improve the modeled distribution of ΔC_{gasex} and residuals in the deep Atlantic and deep Pacific are still high. Thus, a potential mismatch in the seasonality of the air-sea flux and ocean transport is not an explanation for the large residuals.

An intriguing finding of this first set of sensitivity simulations is that the global average air-sea CO_2 flux does not vanish. The inversion yields a global uptake flux of 0.2 GtC yr^{-1} (Table 2). This is inconsistent with the assumption of an ocean in steady state at preindustrial time. We attribute this to the choice of the normalization constant in the computation of ΔC_{gasex}. Following earlier work, the constant has been set to yield an average surface concentration of zero and a whole ocean inventory of the ΔC_{gasex} tracer of around 600 GtC. The implication is that a global uptake of 0.2 GtC yr^{-1} is required in our 3000 year long simulations to match the global ΔC_{gasex} inventory. Non-vanishing global air-to-sea net fluxes, within the range of 0.14 to -0.1 GtC yr^{-1} across the different ocean transport models, have also been found by *Mikaloff Fletcher et al.* [2007]; they also normalized ΔC_{gasex} to a zero mean surface concentration.

The ΔC_{gasex} field is renormalized to yield a zero ocean inventory to avoid the implicit requirement of a net ocean uptake. This is permissible as ocean tracer transport is described by a set of linear equations and the addition of a constant does not change tracer divergence. As expected, the global net air-sea flux is reduced close to zero in the EnKF (Table 2). Surprisingly, this reduction is almost entirely achieved by an increase in Southern Ocean outgassing by 0.19 GtC yr^{-1}.

In summary, the air-sea flux for the Southern Ocean region appears to be particularly sensitive for the details of the model setup and the ΔC_{gasex} field should preferentially be normalized to yield a zero global inventory. We note that the results presented in the Figures and in Tables 1 and 3 and further discussed below have all been obtained by applying ΔC_{gasex} fields normalized to a zero inventory.

3.2.2. Sensitivity of natural air-sea fluxes to different reconstructions of ΔC_{gasex}

Next, we investigate the sensitivity of the natural air-sea fluxes to the four different ΔC_{gasex} fields. At this stage, we only use the *Standard* circulation setup of the Bern3D model.

The four ΔC_{gasex} reconstructions differ remarkably. The root-mean-square-error (RMSE) between the different ΔC_{gasex} fields ranges from 6.91 μmol l^{-1} (between TTD and CFC) to 13.17 μmol l^{-1} (between TrOCA and CFC). Figure 4 shows the zonally-averaged distribution for each of the four reconstructions in the upper Pacific. Differences are only due to the use of different C_{anth} reconstructions. Large differences in ΔC_{gasex} of order 20 μmol l^{-1} are found in various regions. The TrOCA reconstruction yields higher values in the Pacific equatorial thermocline and lower values in the Pacific AAIW than any of the other three reconstructions. In the North Pacific thermocline around 50^{o}N, ΔC_{gasex} concentrations are higher for the ΔC^* and the TrOCA reconstructions than for the TTD and CFC reconstructions; CFC concentrations suggest the presence of a substantial amount of anthropogenic carbon and thus a relatively low ΔC_{gasex} concentrations in this region.

As with the different circulations, the magnitude of flux in the Southern Ocean, the southern mid-latitudes, and in the high latitude Atlantic are particularly sensitive to the choice of the ΔC_{gasex} fields (Figure 5, Table 2). For all other regions, deviations are less than 0.06 GtC yr^{-1}. Inferred outgassing in the Southern Ocean varies almost by a factor of two for the different reconstructions and ranges from 0.53 (TTD, CFC) to 0.98 GtC yr^{-1} (TrOCA). The TrOCA- and the ΔC^*- based reconstructions yield a higher concentration of C_{anth} and thus a lower ΔC_{gasex} in the AAIW compared to the CFC and TTD reconstructions. This implies a stronger preindustrial Southern Ocean outgassing for the TrOCA and the ΔC^* reconstructions. The TrOCA reconstruction yields also a very high uptake flux in the southern mid-latitude Indian ocean, probably as a result of relatively high ΔC_{gasex} concentrations in SAMW.

It might be instructive to compare the fluxes deduced from the different reconstructions and model setups with those derived from the pCO_2 climatology of *Takahashi et al* [2008]. The TTD-based fluxes show the best agreement in terms of correlation and relative standard deviation with the pCO_2-based fluxes [*Taylor*, 2001]. The CFC estimates yield a larger standard deviation and the ΔC^* and TrOCA estimates also a smaller correlation. Results from the standard circulation setup compare better with the pCO_2-derived fluxes than those from alternative circulation setups (Figure S3).

In conclusion, the explicit consideration of uncertainties in ΔC_{gasex} explains the larger error bars given in this study compared to those estimated by *Gruber et al.* [2009] and *Mikaloff Fletcher et al.* [2007]. Best agreement with the pCO_2-based contemporary fluxes is found for the standard circulation setup and the TTD reconstruction.

3.2.3. Sensitivity of natural air-sea fluxes to the inversion method

The Green's function of the Bern3D model have also been used in the inversion of *Mikaloff Fletcher et al.* [2007] allowing us to compare the sensitivity of the flux to the choice of inversion method and experimental details. Surprisingly large differences are found given that the same ΔC_{gasex} data calculation and the same ocean model are applied in both inversions (Table 2). Southern Ocean outgassing is 0.4 GtC yr^{-1} larger in the EnKF inversion than in the GFOI. Uptake in the southern mid-latitude Pacific and Indian is also larger in the EnKF inversion, but results are similar for the southern mid-latitude Pacific. The GFOI yields 0.2 GtC yr^{-1} more outgassing in the southern tropical Pacific than the EnKF.

The GFOI yields a relatively low preindustrial uptake flux in the northern high latitude Atlantic and a substantial uptake in the northern mid latitude Atlantic. This has been previously attributed to a tendency of the ocean models applied in the GFOI to produce North Atlantic Deep Water too far south, with little or no formation in the Nordic Seas [*Gruber et al.*, 2009]. However, this shortcoming is not evident in the Bern3D-EnKF inversion that yields no preindustrial uptake flux in the mid latitude North Atlantic and a contemporary northern high-latitude flux that is almost identical to the flux from the pCO_2 climatology (Figure 1).

It is beyond the scope of this study to identify in detail the experimental differences that lead to the different results for the EnKF and the GFOI. However, residuals between assimilated and modeled data may provide an indication (Figure 3 and Figure 7 in *Mikaloff Fletcher et al.* [2007]). Both inversions yield substantial root mean square deviations between assimilated and optimized ΔC_{gasex} for all ocean models and for all experimental setups. The inversions yield a smoother distribution in ΔC_{gasex} with weaker gradients than reconstructed. We have implemented the fluxes from the GFOI in a forward simulation with the Bern3D model and found a root mean square deviation between reconstructed and simulated ΔC_{gasex} field of 18.7 μmol l^{-1} compared to the 16.86 μmol l^{-1} for EnKF inversion. The difference is likely explained by different weighting of the assimilated data in the GFOI and the EnKF and should not be interpreted as an indication for the quality of the two inversions. Both inversions have difficulties to represent the reconstructed ΔC_{gasex} and the qualitatively similar flux patterns of the EnKF and of the GFOI yield similar root mean square deviations.

3.2.4. Deviations between assimilated and modeled ΔC_{gasex} concentrations

The RMSE between the reconstructed and modeled ΔC_{gasex} fields are large for all setups (Table 2, 3). RMSE are between 18 (standard) and 14 μmol l^{-1} ("PSI $\times$ 3") for different circulations and between 16 (standard) and 20 μmol l^{-1} for the different ΔC_{gasex} reconstruction and standard circulation. The zonally-averaged residuals in the Atlantic, Pacific and Indian range between -40 and +40 μmol l^{-1}, comparable to reconstructed ΔC_{gasex} range of -60 to +60 μmol l^{-1} (Figure 3). Part of the data-model mismatch is very likely related to deficiencies in the Bern3D transport. Most notable is a too weak formation and northward penetration of AAIW and a too shallow penetration of NADW in the standard setup. However, large residuals and RMSE are not unique to the Bern3D-EnKF assimilation, but have also been found for each of the ten model or model versions used by *Mikaloff Fletcher et al.* [2007] with a reported RMSE range between 16 and 21 μmol kg^{-1}. These large residuals may point to some fundamental problems with the ΔC_{gasex} tracer.

ΔC_{gasex} is advected and mixed from the surface and has no sources and sinks in the interior ocean implying that concentrations in the interior should be within the concentration range of the source regions. However, interior concentrations often appear to be outside the concentration range of potential source regions. For the ΔC^* reconstruction, concentrations are below 40 μmol l^{-1} between 500 and 1000 m, whereas higher concentrations (up to 68 μmol l^{-1}) are again found at greater depths in the North Atlantic. The relatively high concentrations in the thermocline and the deep northern Pacific in the ΔC^* reconstruction appear also not to be reflected in any of the potential source waters. Concentrations in the deep ($>$ 2000 m) Pacific are up to 35 μmol l^{-1}, whereas concentrations in the Southern Ocean surface and in the deep Indian and in the Atlantic sector of the Southern Ocean are clearly lower. Similarly, the relatively high values of 5 μmol l^{-1} in the upper thermocline around 35^{o}S in the Indian and Atlantic appear to have no correspondence in adjacent source regions. As a consequence, the assimilation is not able to match the ΔC_{gasex} concentrations simultaneously. Data-model misfits are also found in the GFOI of *Mikaloff Fletcher et al.* [2007].

How can these apparent inconsistencies in ΔC_{gasex} be explained? Non-representative sampling may add uncertainties, but we rely on around 47'000 samples to yield 15897 data points on the Bern3D model grid. Analytical uncertainties in the measurements of

C_T, Alk, and PO_4^{3-} are too small and uncertainties in the reconstructed C_{anth} fields can also not explain the data-model mismatch. Potentially important are uncertainties in the Redfield factors used in equation 1. For example, typical concentrations of PO_4^{3-} in the North Pacific are around 3 μmol l^{-1}. A decrease in ($R_{C:P}$+0.5×$R_{N:P}$), used in equation 1, by 10% yields an increase in ΔC_{gasex} of 37 μmol l^{-1}. Alternatively, interior concentrations outside the source region range may be a consequence of past variability in air-sea CO_2 fluxes or ocean transport, e.g. in response to volcanic eruptions or as part of the internal climate variability [*Frölicher et al.*, 2009].

In summary, large residuals are found for all individual setups. This may point to fundamental problems with the ΔC_{gasex} tracer, possibly related to spatial variations in the Redfield ratio between PO_4^{3-} and C_T of order 5 to 10 percent or related to ocean variability.

3.2.5. Meridional ocean carbon transport

Meridional ocean transport rates are linked to the pattern of air-sea gas exchange of CO_2. For the preindustrial steady-state the net air-sea flux corresponds to the divergence in transport. The southward transport increases steadily from the northern high latitudes to reach 0.6 GtC yr^{-1} at 19^{o}N. In other words, the temperate and high-latitude Northern Hemisphere ocean absorbs on average 0.6 GtC yr^{-1} at preindustrial times. Maxima in equatorwards-directed ocean transport are 0.6 GtC yr^{-1} and 0.3 GtC yr^{-1} in the Northern and Southern Hemisphere, supporting a tropical outgassing of 0.9 GtC yr^{-1}. Transport across the equator is small (0.24 GtC yr^{-1}). The carbon uptake in the southern mid-latitudes is reflected in the decrease in northward transport by 0.84 GtC yr^{-1} from 19^{o}S to 44^{o}N. The outgassing of the Southern Ocean is supported by a corresponding preindustrial southward transport.

For the individual basins, we infer an extensive preindustrial southwards transport of CO_2 throughout the Atlantic (Table S1 and Figure 6), whereas transport rates are equatorwards in the Indo-Pacific (north of 40^{o}S). The southward transport in the Atlantic is mainly driven by the formation and export of NADW. In the upper Atlantic ($>$ 1000 meter) carbon transport is directed polewards in the northern high and mid latitudes.

The transport of anthropogenic carbon is primarily northwards. The most important transport pathway is from the Southern Ocean to the mid-latitudes and subtropics in connection with the northward spreading of AAIW and Subantarctic Mode Water, while transport rates are somewhat smaller in the Northern Hemisphere. A substantial fraction of the anthropogenic carbon taken up in the Southern Ocean is exported to the mid-latitudes.

Contemporary meridional ocean carbon transport is directed southwards in the Northern Hemisphere and south of 42^{o}S, and northwards in the temperate and tropical Southern Hemisphere (Figure 6). The large transport of carbon into the Southern Ocean inferred for the preindustrial state is largely offset by the northward transport of anthropogenic carbon and reduced by about a factor of three. Here, we neglect any possible contribution from river-derived carbon.

The spread in transport among the different reconstruction methods is small in the tropical regions (0.05 GtC yr^{-1}), but large for the transport from the southern mid latitudes to the Southern Ocean. The range in the contemporary flux into the Southern Ocean region is from zero flux to 0.33 GtC yr^{-1} across the four different input data sets. The range (0.54 to 0.98 GtC yr^{-1}) is even larger for the preindustrial flux.

In summary, we infer relatively modest meridional transport rates for both the preindustrial and the contemporary ocean and a small carbon transport across the equator. The preindustrial carbon transport into the Southern Ocean is partly offset by the export of anthropogenic carbon out of the Southern Ocean.

4. Discussion and Conclusion

An Ensemble Kalman Filter is combined with the Bern3D ocean model and tracer data to quantify preindustrial, anthropogenic, and contemporary air-sea fluxes of CO_2 and meridional carbon transport within the ocean. We find a substantial preindustrial outgassing in the tropical and in the Southern Ocean, and carbon uptake in the mid - and northern high latitudes as well as a small interhemispheric carbon transport. The anthropogenic carbon uptake offsets the preindustrial net sea-to-air CO_2 flux in the Southern Ocean, implying that the Southern Ocean is currently on average a weak carbon sink for the atmosphere. The reconstructed contemporary fluxes for broad latitudinal bands are largely consistent with results from Green's function ocean inversions [*Gloor et al.*, 2003; *Jacobson et al.*, 2007; *Gruber et al.*, 2009], the fluxes computed from the surface ocean pCO_2 climatology [*Takahashi et al*, 2008], and atmospheric inversions [*Baker et al*, 2006]. However, sensitivity simulations and the analysis of deviations between assimilated and optimized tracer fields reveal large uncertainties in regional air-sea flux, in particular for the Southern Ocean. Improvements in quantification and understanding of Southern Ocean processes is high on the research agenda as this region plays a critical role for the fate of anthropogenic carbon and for the glacial-interglacial CO_2 variations.

The reconstruction of anthropogenic carbon is a potential source of biases in the estimates of ΔC_{gasex}. Another bias may be imposed by the normalization of the ΔC_{gasex} field. We recommend to normalize the ΔC_{gasex} reconstruction to a zero mean ocean inventory instead to a zero mean surface concentration to avoid non-vanishing global air-sea fluxes in the assimilation of ΔC_{gasex} data. Regional air-sea fluxes from the EnKF assimilations are compared to those inferred from observations of the air-sea CO_2 partial pressure differences [*Takahashi et al*, 2008]. Overall, best agreement is found when relying on the TTD reconstruction [*Waugh et al.*, 2006] in the EnKF assimilation. The explicit consideration of uncertainties in the reconstructions of C_{anth} and ΔC_{gasex} explains the larger error bars given in this study compared to those estimated by *Gruber et al.* [2009] and*Mikaloff Fletcher et al.* [2007].

Optimized air-sea fluxes are also sensitive to the choice of the inversion method. For example, preindustrial outgassing in the Southern Ocean is with 0.7 GtC yr^{-1} more than twice as large in the EnKF inversion than in the corresponding Green's function inversion when applying the same ocean model and ΔC_{gasex} data calculation. This suggests that the air-sea fluxes are not tightly constrained by the assimilated data and details of the inversion methods matter.

Large root mean square deviations between the assimilated and the optimized ΔC_{gasex} fields of 15 to 20 μmol l^{-1} are found for all individual setups of this study or by *Mikaloff Fletcher et al.* [2007] who applied ten different models and model versions in their Green's function inversion. The range of zonal mean residuals in ΔC_{gasex} is comparable to the reconstructed range in ΔC_{gasex}. The inversions yield a much smoother distribution in ΔC_{gasex} and gradients are much weaker than reconstructed. This may point to fundamental problems with the ΔC_{gasex} tracer, possibly related to spatial variations in the stochiometric ratios between phosphate and carbon of order 5 to 10 percent or related to ocean variability. These two factors should be more explicitly addressed in future work.

In conclusion, oceanic tracer data have been successfully assimilated with an Ensemble Kalman Filter to quantify regional air-sea fluxes and meridional ocean transport of carbon. Results for the Southern Ocean, southern mid-latitudes and the northern North Atlantic regions are particularly sensitive to uncertainties in input data, to uncertainties in ocean transport, and to the choice of inverse method and experimental details. Systematic differences in assimilated and optimized ΔC_{gasex} fields remain uncomfortably large, suggesting that the error estimates given in this study represent lower bounds. The contemporary, anthropogenic, and preindustrial air-sea CO_2 flux in the Southern Ocean remain uncertain.

Acknowledgments. This study was financially supported by the European Union through the Integrated Project CarboOcean(511106-2), the Swiss National Science Foundation, and the Swiss Staatsekretariat für Bildung und Forschung (#C07.0068; COST Action 735).

References

Álvarez, M., C. Lo Monaco, T. Tanhua, A. Yool, A. Oschlies, J. L. Bullister, C. Goyet, N. Metzl, F. Touratier, E. McDonagh, and H. L. Bryden, Estimating the storage of anthropogenic carbon in the subtropical indian ocean: a comparison of five different approaches, *Biogeosciences Discussions*, *6*(1), 729–796, 2009.

Anderson, L. A., and J. L. Sarmiento, Redfield ratios of remineralization determined by nutrient data analysis, *Global Biogeochemical Cycles*, *8*(1), 65–80, 1994.

Baker, D. F., et al, Transcom 3 inversion intercomparison: Impact of transport model errors on the interannual variability of regional CO_2 fluxes 1988-2003, *Global Biogeochemical Cycles*, *20*(GB1002,), doi:10.1029/2004GB002439, 2006.

Bakker, D., J. Etcheto, J. Boutin, and L. Merlivat, Variability of surface water fCO_2 during seasonal upwelling in the equatorial Atlantic Ocean as observed by a drifting buoy, *Journal of Geophysical Research*, *106*(C5), 9241–9253, 2001.

C. Rödenbeck, C., C. Le Quéré, M. M. Heimann, and R. F. Keeling, Interannual variability in oceanic biogeochemical processes inferred by inversion of atmospheric $O_2/N_2$and CO_2data, *Tellus B*, *60*(5), 685–705, 2008.

Chen, C. T. A., and F. J. Millero, Gradual increase of oceanic CO_2, *Nature*, *277*, 205–206, 1979.

Denman, K. L., G. Brasseur, A. Chidthaisong, P. Ciais, P. M. Cox, R. E. Dickinson, D. Hauglustaine, C. Heinze, E. Holland, D. Jacob, U. Lohmann, S. Ramachandran, P. L. da Silva Dias, S. C. Wofsy, and X. Zhang, Couplings between changes in the climate system and biogeochemistry, in *Climate Change 2007: The Physical Science Basis. Working Group I Contribution to the Fourth Assessment Report of the Intergovernmental Panel on Climate Change*, edited by S. Solomon, D. Qin, M. Manning, Z. Chen, M. Marquis, K. B. Averyt, M. Tignor, and H. L. Miller, pp. 499–588, Cambridge University Press, Cambridge, United Kingdom and New York, NY, USA, 2007.

Edwards, N. R., and R. Marsh, Uncertainties due to transport-parameter sensitivity in an efficient 3-d ocean-climate model, *Climate Dynamics*, *24*(4), 415–433, doi: 10.1007/s00382-004-0508-8, 2005.

Enting, I. G., and J. V. Mansbridge, Seasonal Sources and Sinks of Atmospheric CO_2: Direct Inversion of Filtered Data., *Tellus*, *41B*(2), 11–126, 1989.

Evensen, G., The Ensemble Kalman Filter: theoretical formulation and practical implementation, *Ocean Dynamics*, *53*, 343–367, 2003.

Evensen, G., Sampling strategies and square root analysis schemes for the EnKF, *Ocean Dynamics*, *54*, 539–560, 2004.

Frölicher, T. L., F. Joos, G.-K. Plattner, M. Steinacher, and S. C. Doney, Natural variability and anthropogenic trends in oceanic oxygen in a coupled carbon cycle-climate model ensemble, *Global Biogeochemical Cycles*, *23*(GB1003), doi:10.1029/2008GB003316, 2009.

Gerber, M., F. Joos, M. Vázquez Rodríguez, F. Touratier, and C. Goyet, Regional air-sea fluxes of anthropogenic carbon inferred with an Ensemble Kalman Filter, *Global Biogeochemical Cycles*, *in press*, 2008.

Gloor, M., N. Gruber, J. L. Sarmiento, C. L. Sabine, R. A. Feely, and C. Rödenbeck, A first estimate of present and preindustrial air-sea CO_2 flux patterns based on ocean interior carbon measurements and models, *Geophysical Research Letters*, *30(1)*(1010), 767–782, doi:10.1029/2002GL015594, 2003.

Gruber, N., J. Sarmiento, and T. F. Stocker, An improved method for detecting anthropogenic CO_2 in the oceans, *Global Biogeochemical Cycles*, *10*(4), 809–837, 1996.

Gruber, N., M. Gloor, S. Mikaloff Fletcher, S. Doney, S. Dutkiewicz, M. Follows, M. Gerber, A. Jacobson, F. Joos, K. Lindsay, D. Menemenlis, A. Mouchet, S. Müller, J. Sarmiento, and T. Takahashi, Oceanic sources, sinks, and transport of atmospheric CO_2, *Global Biogeochemical Cycles*, *23*(GB1005), doi:10.1029/2008GB003349, 2009.

Heimann, M., and E. Maier-Reimer, On the Relations Between the Oceanic Uptake of CO_2 and Its Carbon Isotopes, *Global Biogeochemical Cycles*, *10*(1), 89–110, 1996.

Jacobson, A. R., S. E. Mikaloff Fletcher, N. Gruber, J. L. Sarmiento, and M. Gloor, A joint atmosphere-ocean inversion for surface fluxes of carbon dioxide: 1. methods and global-scale fluxes, *Global Biogeochem. Cycles*, *21*(GB1019,), doi:10.1029/2005GB002556, 2007.

Joos, F., and R. Spahni, Rates of change in natural and anthropogenic radiative forcing over the past 20,000 years, *Proceedings of the National Academy of Sciences of the United States of America (PNAS)*, *105*(5), 1425–1430, 2008.

Kaminski, T., M. Heimann, P. Peylin, P. Bousquet, and P. Ciais, Inverse modeling of atmospheric carbon dioxide fluxes, *Science*, *294*(5541), 259, doi:10.1126/science.294.5541.259a, 2001.

Key, R. M., A. Kozyr, C. L. Sabine, K. Lee, R. Wanninkhof, J. L. Bullister, R. A. Feely, F. J. Millero, C. Mordy, and T.-H. Peng, A global ocean carbon climatology: Results from Global Data Analysis Project (GLODAP), *Global Biogeochem. Cycles*, *18*(GB4031), doi:10.1029/2004GB002247, 2004.

Lüthi, D., M. Le Floch, B. Bereiter, T. Blunier, J.-M. Barnola, U. Siegenthaler, D. Raynaud, J. Jouzel, H. Fischer, K. Kawamura, and T. F. Stocker, High-resolution carbon dioxide concentration record 650,000-800,000 years before present, *Nature*, *453*, 379–

382, doi:10.1038/nature06949, 2008.

Maier-Reimer, E., Geochemical Cycles in an Ocean General Circulation Model. Preindustrial Tracer Distributions, *Global Biogeochemical Cycles*, *7*(3), 645–677, 1993.

Matear, R. J., C. S. Wong, and L. Xie, Can CFCs be used to determine anthropogenic CO_2?, *Global Biogeochemical Cycles*, *17*(1013), doi:10.1029/2001GB001415, 2003.

Matsumoto, K., and N. Gruber, How accurate is the estimation of anthropogenic carbon in the ocean? an evaluation of the ΔC^* method, *Global Biogeochemical Cycles*, *19*, doi:10.1029/2004GB002397, 2005.

Mikaloff Fletcher, S. E., N. Gruber, A. R. Jacobson, S. C. Doney, S. Dutkiewicz, M. Gerber, M. Follows, F. Joos, K. Lindsay, D. Menemenlis, A. Mouchet, S. A. Müller, and J. L. Sarmiento, Inverse estimates of anthropogenic CO_2 uptake, transport, and storage by the ocean, *Global Biogeochemical Cycles*, *20*(GB2002), doi:10.1029/2005GB002530, 2006.

Mikaloff Fletcher, S. E., N. Gruber, A. R. Jacobson, M. Gloor, S. C. Doney, S. Dutkiewicz, M. Gerber, M. Follows, F. Joos, K. Lindsay, D. Menemenlis, A. Mouchet, S. A. Müller, and J. L. Sarmiento, Inverse estimate of the oceanic sources and sinks of natural CO_2 and the implied oceanic carbon transport, *Global Biogeochemical Cycles*, *27*(GB1010), doi:10.1029/2006GB0027, 2007.

Müller, S. A., F. Joos, N. R. Edwards, and T. F. Stocker, Water mass distribution and ventilation time scales in a cost-efficient, three-dimensional ocean model, *Journal of Climate*, *19*(21), 5479–5499, 2006.

Müller, S. A., F. Joos, G.-K. Plattner, N. R. Edwards, and T. F. Stocker, Modeled natural and excess radiocarbon: Sensitivities to the gas exchange formulation and ocean transport strength, *Global Biogeochemical Cycles*, *22*(GB3011), doi:10.1029/2007GB003065, 2008.

Murnane, R., J. Sarmiento, and C. LeQuéré, Spatial Distribution of Air-Sea CO_2 Fluxes and the Interhemispheric Transport of Carbon by the Oceans, *Global Biogeochemical Cycles*, *13*(2), 287–305, 1999.

Parekh, P., F. Joos, and S. A. Müller, A modeling assessment of the interplay between aeolian iron fluxes and iron-binding ligands in controlling carbon dioxide fluctuations during Antarctic warm events, *Paleoceanography*, *23*(PA4202), doi:10.1029/2007PA001531, 2008.

Sabine, C. L., R. A. Feely, N. Gruber, R. M. Key, K. Lee, J. L. Bullister, R. Wanninkhof, C. S. Wong, D. W. R. Wallace, B. Tilbrook, F. J. Millero, T.-H. Tsung-Hung Peng, A. Kozyr, T. Ono, and A. F. Ríos, The oceanic sink for anthropogenic CO_2, *Science*, *305*(5682), 367 – 371, doi:10.1126/science.1097403, 2004.

Sarmiento, J., P. Monfray, E. Maier-Reimer, O. Aumont, R. Murnane, and J. Orr, Sea-air CO_2 Fluxes and Carbon Transport: A Comparison of Three Ocean General Circulation Models, *Global Biogeochemical Cycles*, *14*(4), 1267–1281, 2000.

Sarmiento, J. L., and N. Gruber, Chapter 8: Carbon Cycle, in *Ocean biogeochemical dynamics*, pp. 318–358, Princeton University Press, 2006.

Sarmiento, J. L., and E. T. Sundquist, Revised budget for the oceanic uptake of anthropogenic carbon dioxide, *Nature*, *536*, 589–593, doi:10.1038/356589a0, 1992.

Schlitzer, R., Carbon export fluxes in the Southern Ocean: results from inverse modeling and comparison with satellite-based estimates, *Deep Sea Research Part II*, *49*, 1623–1644, 2002.

Schlitzer, R., Assimilation of radiocarbon and chlorofluorocarbon data to constrain deep and bottom water transports in the world ocean, *Journal of Physical Oceanography*, *37*(2), 259–276, 2007.

Takahashi, T., et al, Climatological mean and decadal changes in surface ocean pCO_2, and net sea-air CO_2 flux over the global oceans, *Deep Sea Res. II*, *in press*, doi: doi:10.1016/j.dsr2.2008.12.009, 2008.

Takahashi, T., S. C. Sutherland, C. Sweeney, A. Poisson, N. Metzl, B. Tilbrook, N. Bates, R. Wanninkhofe, R. A. Feely, C. Sabine, J. Olafsson, and Y. Nojiri, Global sea-air CO_2 flux based on climatological surface ocean pco2, and seasonal biological and temperature effects, *Deep Sea Research Part II*, *49*, 1601–1622, 2002.

Tans, P. P., I. Y. Fung, and T. Takahashi, Observational contraints on the global atmospheric CO_2 budget, *Science,*, *247*, 1431–1439, doi:10.1126/science.247.4949.1431, 1990.

Taylor, K. E., Summarizing multiple aspects of model performance in a single diagram, *Journal of Geophysical Research*, *106*(D7), 7183–7192, 2001.

Thomas, H., and V. Ittekkot, Determination of anthropogenic CO_2 in the North Atlantic Ocean using water mass ages and CO_2 equilibrium chemistry, *Journal of Marine Systems*, *27*, 325–336(12), doi:10.1016/S0924-7963(00)00077-4, 2001.

Touratier, F., and C. Goyet, Definition, properties, and Atlantic Ocean distribution of the new tracer TrOCA, *Journal of Marine System*, *46*, 169–179, 2004.

Touratier, F., L. Azouzi, and C. Goyet, CFC-11, 14C and 3H tracers as a means to assess anthropogenic co2 concentrations in the ocean, *Tellus B*, *59*, 318–325, doi: 10.1111/j.1600-0889.2006.00247.x, 2007.

Tschumi, T., F. Joos, and P. Parekh, How important are Southern Hemisphere wind changes for low glacial carbon dioxide? A model study, *Paleoceanography*, *23*(PA4208), doi:10.1029/2008PA001592, 2008.

Vázquez Rodríguez, M., F. Touratier, C. LoMonaco, D. W. Waugh, X. A. Padin, R. J. Bellerby, C. Goyet, N. Metzel, A. F. Ríos, and F. F. Perez, Anthropogenic carbon distributions in the Atlantic Ocean: data-based estimates from the Arctic to the Antarctic, *Biogeosciences*, *6*, 439–451, 2009.

Volk, T., and M. I. Hoffert, Ocean carbon pumps: analysis of relative strengths and efficiencies in ocean-driven atmospheric CO_2 changes, in *The Carbon Cycle and Atmospheric CO_2: Natural Variations Archean to Present*, edited by E. T. Sundquist and W. S. Broecker, Geophysical Monograph 32, pp. 99–110, American Geophysical Union, Washingto, D.C, 1985.

Wanninkhof, R., Relationship between wind speed and gasexchange over the ocean, *Journal of Geophysical Research*, *97*, 7373–7382, 1992.

Waugh, D. W., T. W. N. Haine, and T. M. Hall, Transport times and anthropogenic carbon in the subpolar North Atlantic Ocean, *Deep Sea Research Part I*, *51*(11), 1475–1491, doi:10.1016/j.physletb.2003.10.071, 2004.

Waugh, D. W., T. M. Hall, B. I. McNeil, R. Key, and R. Matear, Anthropogenic CO_2 in the oceans estimated using transit-time distributions, *Tellus*, *58B*, 376–390, doi:10.1111/j.1600-0889.2006.00222.x., 2006.

Table 1. Regional net air-to-sea fluxes of CO_2 for the anthropogenic perturbation, the preindustrial time, and the present in GtC yr^{-1}. Fluxes of this study are compared to those from the ocean inversion of *Mikaloff Fletcher et al.* [2006, 2007] and those derived from a climatology of the air-sea CO_2 partial pressure difference [*Takahashi et al*, 2008] as published by *Gruber et al.* [2009]. Fluxes of this study represent weighted averages of the fluxes shown in Table 3 for four different reconstructions of C_{ant} and C_{gasex}. Uncertainties represent ±1 standard deviation. Uncertainties for this study include those from uncertainties in input data, ocean transport, and river-driven outgassing

Region	This study			Mikloff Fletcher et al. 2007			Takahashi et al. 2008
	C_{anth}	Natural	Total	C_{anth}	Natural	Total	Total
Atlantic N.High Lat.	0.13 ± 0.06	0.16± 0.04	0.25 ± 0.07	0.09 ± 0.04	0.11 ± 0.02	0.17 ± 0.06	0.25
Atlantic N. Mid Lat.	0.10 ±0.05	0.02± 0.05	0.11 ± 0.06	0.13 ± 0.04	0.12 ± 0.04	0.24 ± 0.06	0.15
Atlantic N. Low Lat.	0.04 ± 0.05	0.16± 0.04	0.16 ± 0.06	0.04 ± 0.04	0.08 ± 0.04	0.08 ± 0.06	0.05
Atlantic N. Tropics	0.03 ± 0.02	-0.11± 0.02	-0.17 ± 0.05	0.04 ± 0.02	-0.03 ± 0.01	-0.08 ± 0.05	-0.03
Atlantic S. Tropics	0.11± 0.03	-0.09±0.02	0 ± 0.04	0.09 ± 0.02	-0.14 ± 0.02	-0.06 ± 0.03	-0.09
Atlantic S. Low Lat.	0±0.01	0±0.01	0 ± 0.01	0.02 ± 0.01	-0.02 ± 0.01	0.01 ± 0.01	-0.02
Atlantic S. Mid Lat.	0.05±0.04	0.17±0.08	0.19 ± 0.08	0.05 ± 0.02	0.11 ± 0.05	0.16 ± 0.05	0.13
Pacific N. High Lat.	0.05±0.03	0 ± 0.04	0.02± 0.05	0.04 ± 0.01	-0.02 ± 0.04	0± 0.04	0.12
Pacific N. Mid Lat.	0.05±0.06	0.25±0.06	0.35 ± 0.08	0.15 ± 0.04	0.31 ± 0.05	0.42 ± 0.07	0.37
Pacific N. Tropics	0.18± 0.05	-0.30±0.06	-0.15 ± 0.08	0.18 ± 0.04	-0.22 ± 0.06	-0.06 ± 0.07	-0.12
Pacific S. Tropics	0.12± 0.05	-0.25±0.08	-0.14 ± 0.10	0.11 ± 0.02	-0.41 ± 0.08	-0.31 ± 0.09	-0.32
Pacific S. Mid Lat.	0.09±0.06	0.52±0.10	0.61 ± 0.11	0.11 ± 0.04	0.36 ± 0.09	0.46 ± 0.10	0.28
Indian Tropics	0.07±0.04	-0.12±0.03	-0.14 ± 0.06	0.11 ± 0.03	-0.14 ± 0.02	-0.12 ± 0.06	-0.13
Indian S. Mid Lat.	0.12± 0.12	0.29±0.12	0.40 ± 0.09	0.25 ± 0.08	0.22 ± 0.06	0.46 ± 0.09	0.37
Polar and Subpolar Ocean	0.86 ± 0.25	-0.69±0.15	0.15 ± 0.25	0.74 ± 0.17	-0.40 ± 0.11	0.34 ± 0.20	0.30
Global	2.10± 0.30	-0.01±0.09	1.67 ± 0.38	2.18 ± 0.25	-0.05 ± 0.08	1.70 ± 0.35	1.31

Table 2. Regional net air-to-sea fluxes in GtC yr^{-1} of natural (preindustrial without river-derived) CO_2 for four different Bern3D transport versions and two modified setups with the standard Bern3D model. The root mean square error (RMSE) between optimized and data-based fields of C_{gasex} are calculated using all data points assimilated to the optimization. The column "zero inventory" shows the air-sea fluxes inferred from the ΔC^* reconstruction with an offset such that the total inventory of the ΔC_{gasex} is zero (see equation 1). The "seasonally forced" column shows air-sea fluxes with a modified flux pattern in the northern high Atlantic and Southern Ocean to increase the uptake during the winter months. The "Ocean Inversion" column shows the results from the Bern3D model in *Mikaloff Fletcher et al.* [2007]

Region	Area in $10^6 km^2$	Standard	ACC ×3	PSI ×3	High Diffusion	Seasonally Forced	zero Inventory	Ocean Inversion
Atlantic N.High Lat.	9.45	0.21	0.32	0.43	0.21	0.12	0.18	0.14
Atlantic N. Mid Lat.	11.81	-0.01	0.10	0.09	0.02	0.07	0	0.09
Atlantic N. Low Lat.	16.53	0.16	0.15	0.14	0.13	0.15	0.15	0.09
Atlantic N. Tropics	14.17	-0.10	-0.11	-0.11	-0.13	-0.09	-0.09	-0.03
Atlantic S. Tropics	10.23	-0.06	-0.09	-0.10	-0.06	-0.10	-0.09	-0.10
Atlantic S. Low Lat.	10.23	0	0	0	0	0	0	-0.01
Atlantic S. Mid Lat.	9.45	0.23	0.14	0.13	0.19	0.09	0.21	0.05
Pacific N. High Lat.	12.20	-0.02	-0.01	0.0	-0.004	-0.02	-0.01	0.01
Pacific N. Mid Lat.	37.78	0.28	0.27	0.28	0.29	0.26	0.25	0.20
Pacific N. Tropics	38.96	-0.28	-0.30	-0.32	-0.35	-0.30	-0.29	-0.18
Pacific S. Tropics	28.33	-0.26	-0.26	-0.26	-0.20	-0.25	-0.24	-0.44
Pacific S. Mid Lat.	39.36	0.45	0.57	0.60	0.46	0.44	0.48	0.47
Indian Tropics	31.88	-0.10	-0.11	-0.12	-0.10	-0.10	-0.11	-0.11
Indian S. Mid Lat.	24.01	0.22	0.25	0.27	0.21	0.17	0.26	0.11
Polar and Subpolar Ocean	58.64	-0.53	-0.72	-0.83	-0.47	-0.46	-0.72	-0.32
Global		0.19	0.20	0.20	0.20	-0.02	-0.01	-0.03
RMSE ΔC_{gasex} (μmol l^{-1})		17.82	15.29	14.15	16.94	17.27	16.86	18.7

Table 3. Regional net sea-to-air fluxes in GtC yr^{-1} of natural, anthropogenic and contemporary CO_2 inferred with four different reconstructions of anthropogenic carbon and the ΔC_{gasex} tracer. The contemporary air-sea flux is calculated by adding the river-derived outgassing [*Jacobson et al.*, 2007] to the natural and anthropogenic flux. The skill scores and the RMSE for C_{anth} are taken from *Gerber et al.* [2008].

Region	River Derived	ΔC^*			TTD			TrOCA			CFC		
	Outgassing	C_{anth}	Natural	Total	C_{anth}	Natural	Total	C_{anth}	Natural	Total	C_{anth}	Natural	Total
Atlantic N.High Lat.	-0.03 ± 0.01	0.12	0.18	0.27	0.09	0.16	0.22	0.17	0.16	0.30	0.16	0.11	0.24
Atlantic N. Mid Lat.	-0.01 ± 0.01	0.11	0	0.10	0.08	0.03	0.10	0.15	0	0.14	0.07	0.06	0.12
Atlantic N. Low Lat.	-0.04 ± 0.02	0.04	0.15	0.15	0.06	0.16	0.18	0.01	0.17	0.14	0.06	0.15	0.17
Atlantic N. Tropics	-0.09 ± 0.05	0.03	-0.09	-0.15	0.04	-0.13	-0.18	0.02	-0.10	-0.17	0.03	-0.13	-0.19
Atlantic S. Tropics	-0.02 ± 0.01	0.09	-0.09	-0.02	0.10	-0.09	-0.01	0.15	-0.08	0.05	0.12	-0.10	0
Atlantic S. Low Lat.	0 ± 0	0	0	0	0	0.01	0.01	0.01	-0.01	0	0	0.01	0.01
Atlantic S. Mid Lat.	-0.01 ± 0	0.08	0.21	0.28	0.07	0.09	0.15	-0.01	0.22	0.20	0.08	0.08	0.15
Pacific N. High Lat.	-0.03 ± 0.01	0.05	-0.01	0.01	0.03	0	0	0.10	0	0.07	0.03	0.02	0.02
Pacific N. Mid Lat.	-0.05 ± 0.02	0.14	0.25	0.34	0.17	0.23	0.35	0.08	0.29	0.32	0.21	0.23	0.41
Pacific N. Tropics	-0.03 ± 0.01	0.15	-0.29	-0.17	0.21	-0.29	-0.11	0.15	-0.33	-0.21	0.20	-0.30	-0.13
Pacific S. Tropics	-0.01 ± 0.01	0.07	-0.24	-0.18	0.16	-0.25	-0.10	0.09	-0.24	-0.16	0.16	-0.27	-0.12
Pacific S. Mid Lat.	0 ± 0	0.14	0.48	0.62	0.05	0.50	0.55	0.12	0.58	0.70	0.06	0.54	0.60
Indian Tropics	-0.09 ± 0.04	0.05	-0.11	-0.15	0.06	-0.11	-0.14	0.10	-0.16	-0.15	0.07	-0.11	-0.13
Indian S. Mid Lat.	-0.01 ± 0.00	0.16	0.26	0.41	0.16	0.23	0.38	-0.03	0.46	0.42	0.17	0.24	0.40
Polar and Subpolar Ocean	-0.01 ± 0.00	0.72	-0.72	-0.01	0.75	-0.54	0.20	1.09	-0.98	0.10	0.88	-0.54	0.33
Global	-0.41 ± 0.21	1.95	-0.01	1.53	2.04	0	1.62	2.20	-0.02	1.77	2.30	-0.01	1.88
Skill score		0.839			0.870			0.760			0.686		
RMSE ΔC_{gasex} (μmol l^{-1})			16.86			16.39			19.44			17.21	
RMSE C_{anth} (μmol l^{-1})		7.20			6.76			9.85			13.37		

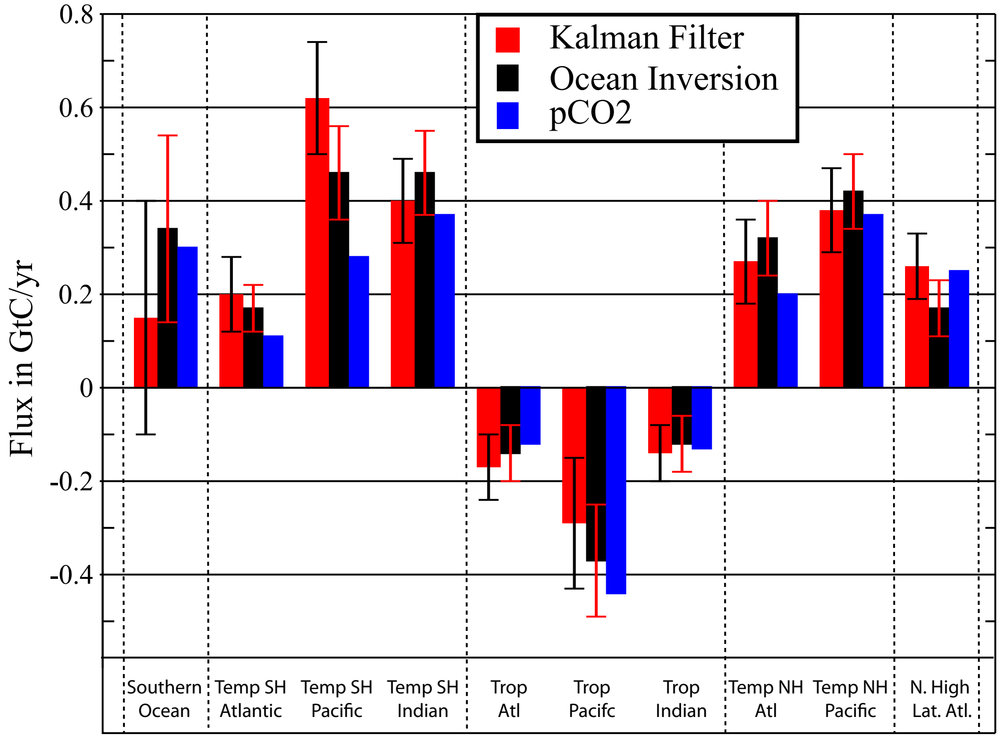

Figure 1. Contemporary net air-to-sea fluxes of CO_2 for aggregated regions as inferred by assimilating ocean tracer data into the Bern3D transport model (red). Error bars represent ± 1 standard deviation and include uncertainties from input data, ocean transport, and river-derived outgassing. Results obtained by the Green's function ocean inversion of *Mikaloff Fletcher et al.* [2006, 2007] (black) and from a climatology of the air-sea CO_2 partial pressure difference [*Takahashi et al*, 2008] as published by *Gruber et al.* [2009] (blue) are shown for comparison.

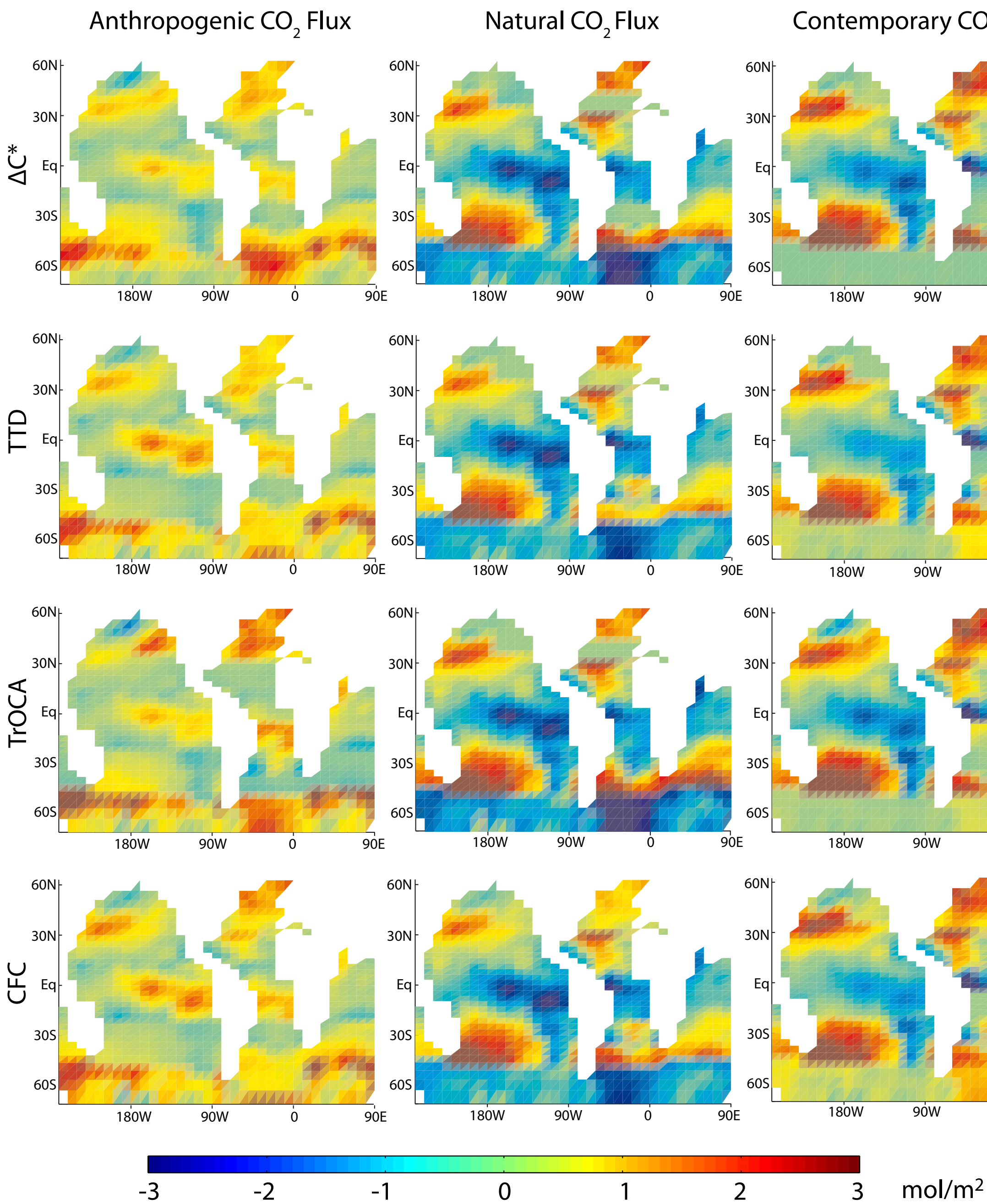

Figure 2. Annual mean net air-to-sea flux (mol m^{-2}) of CO_2 for the anthropogenic perturbation (left), the preindustrial (middle), and the present (1995, right) as inferred by assimilating four different reconstructions of anthropogenic carbon and of ΔC_{gasex} based on the ΔC^{*}, the TTD, the TrOCA, and the CFC methods into the Bern3D model.

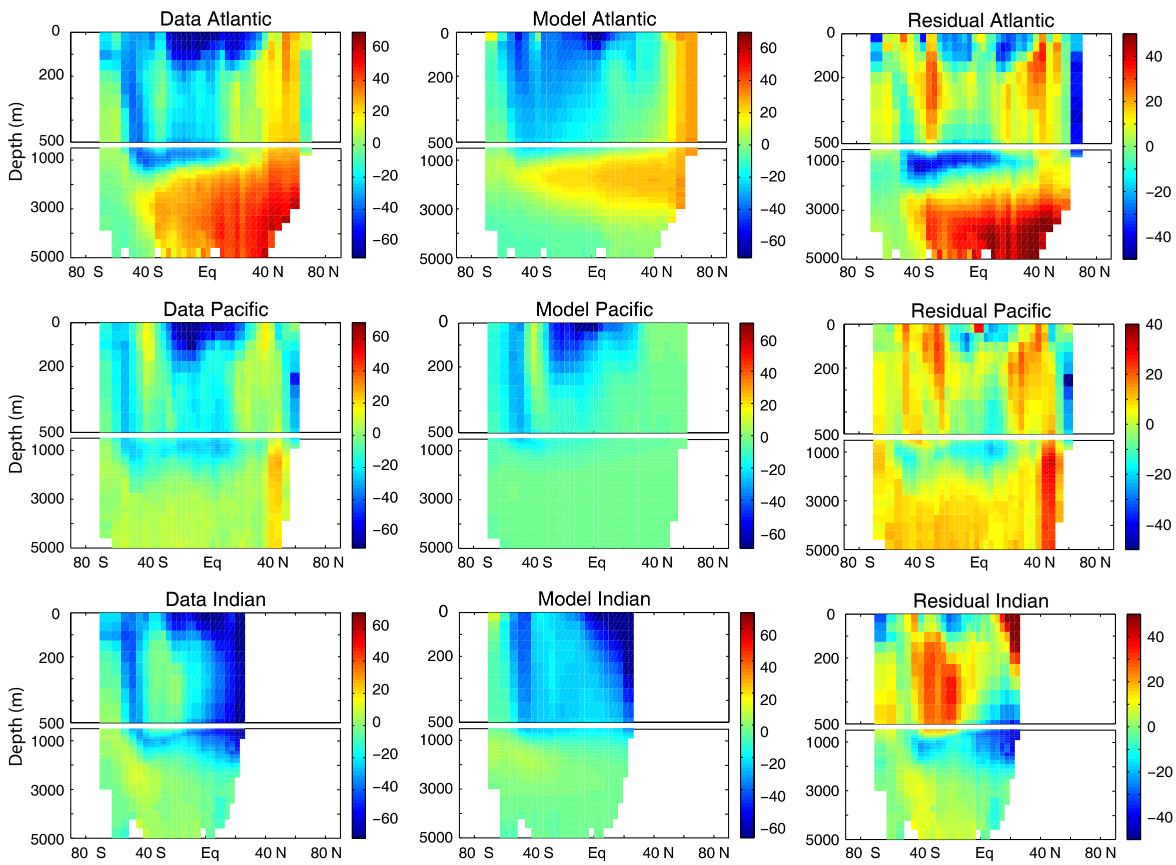

Figure 3. Zonal average of data-based and modeled distribution of ΔC_{gasex} and of the corresponding residuals (data minus model) in μmol l^{-1} for the Atlantic, Pacific, and Indian.

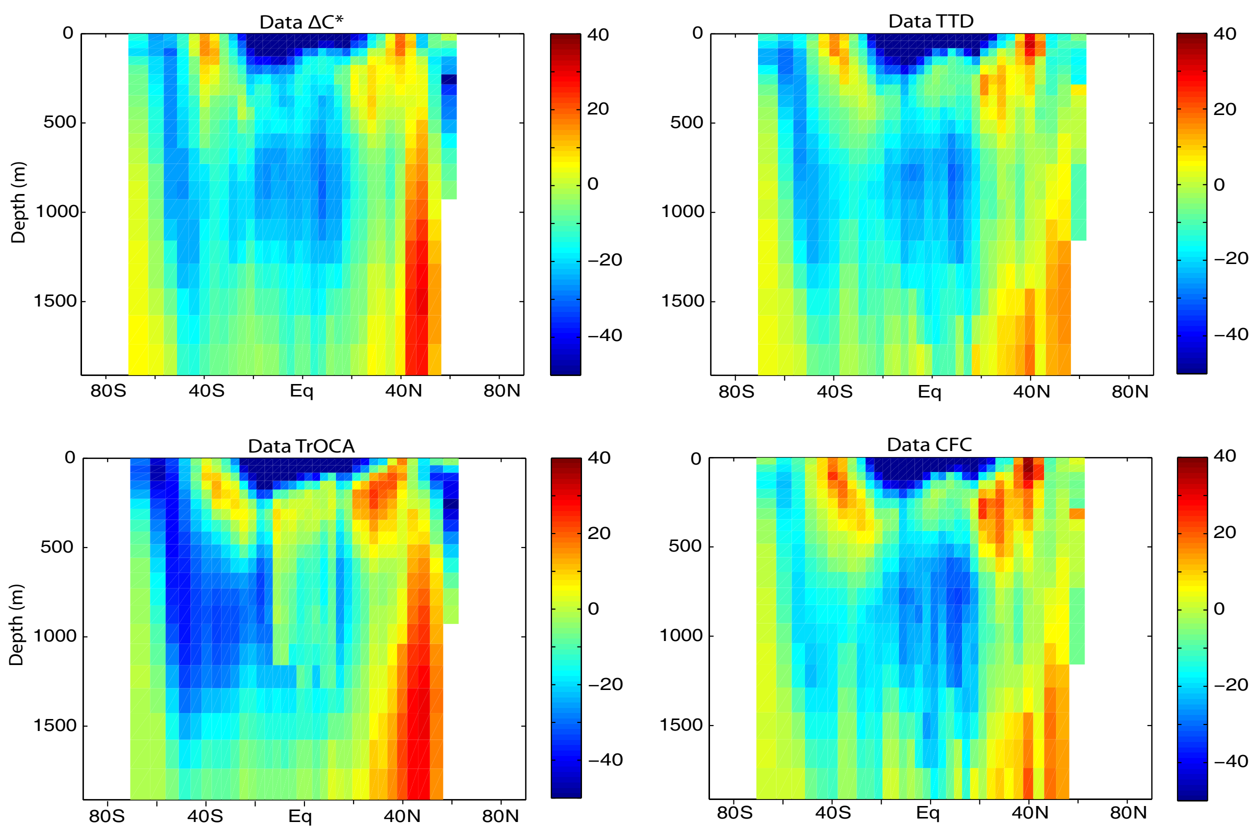

Figure 4. Zonal average of data-based ΔC_{gasex} in μmol l^{-1} in the upper Pacific for four reconstruction methods.

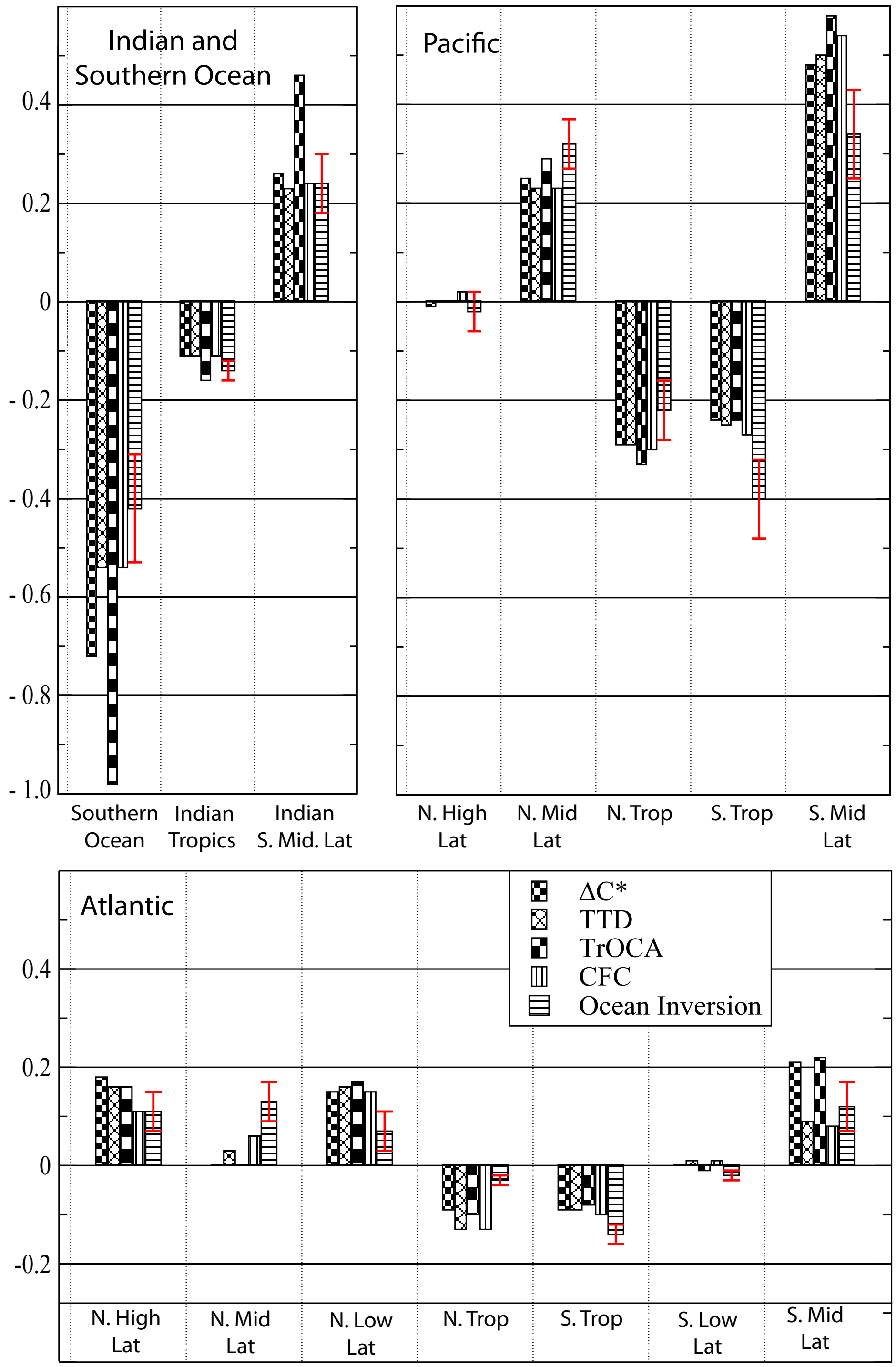

Figure 5. Regional net air-to-sea fluxes in GtC yr^{-1} for four different reconstruction methods compared to the estimates of *Mikaloff Fletcher et al.* [2007]. The error bar shows the weighted standard deviation of the models participating in *Mikaloff Fletcher et al.* [2007].

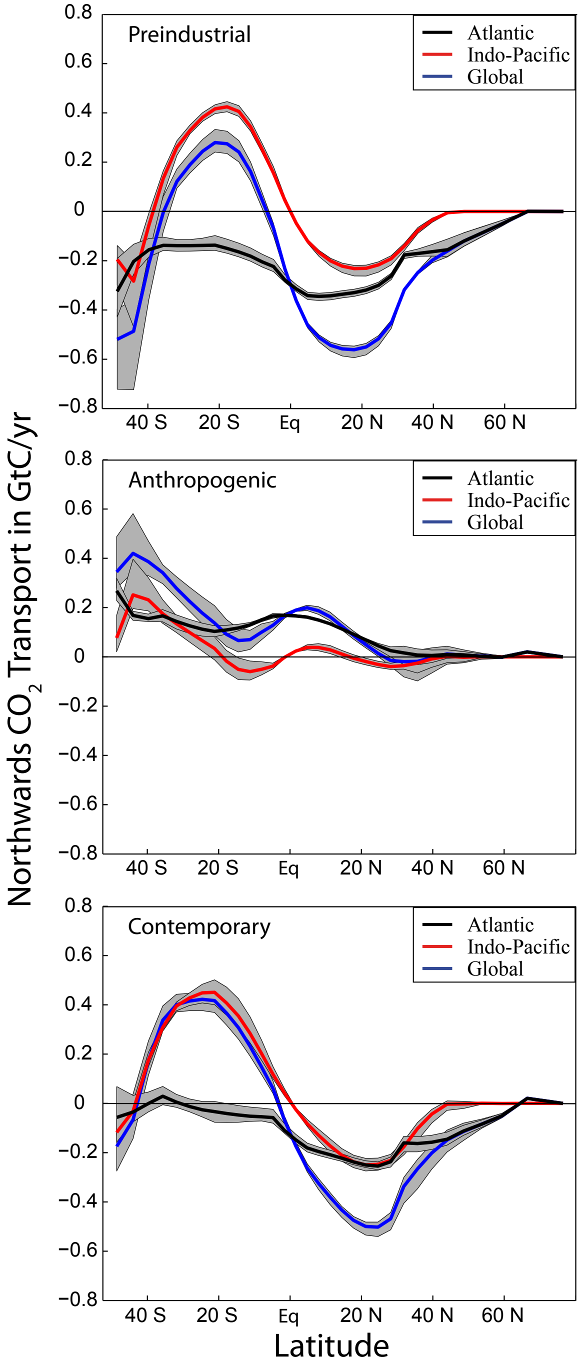

Figure 6. Meridional ocean carbon transport for the (a) preindustrial, (b) the anthropogenic perturbation, and (c) the present for the global ocean (blue), the Atlantic (black) and the Indo-Pacific (red). Rates are inferred by assimilating four different reconstructions of C_{anth} and ΔC_{gasex} into the standard version of the Bern3D model. Solid lines show best estimates and the shading the spread from the different input data.

Carbon sources and sinks from an Ensemble Kalman Filter ocean data assimilation. Supplemental material

M. Gerber

Climate and Environmental Physics, Physics Institute, University of Bern,

3012 Bern, Switzerland.

F. Joos

Climate and Environmental Physics, Physics Institute, University of Bern,

3012 Bern, Switzerland and Oeschger Centre for Climate Change Research,

University of Bern.

References

Takahashi, T., et al, Climatological mean and decadal changes in surface ocean pCO_2, and net sea-air CO_2 flux over the global oceans, *Deep Sea Res. II*, *in press*, doi: doi:10.1016/j.dsr2.2008.12.009, 2008.

M.Gerber, Climate and Environmental Physics, Physics Institute, University of Bern, 3012 Bern, Switzerland. (mgerber@climate.unibe.ch)

Table 1. Supplement material Table S1: Meridional transport rates in GtC yr^{-1} for the different data-based estimates. A positive sign indicates a southwards transport. The flux is across the southern border of each region. The values in parentheses represent the net eastward flux across the eastern border of the box. A negative sign represents a westward flux.

Region	*Meridional transport in GtC yr^{-1}*			
	TTD	CFC	TrOCA	ΔC^*
Atlantic N.High Lat. (46 N)	0.16	0.11	0.16	0.18
Atlantic N. Mid Lat. (34 N)	0.19	0.17	0.17	0.18
Atlantic N. Low Lat. (16 N)	0.35	0.32	0.34	0.33
Atlantic N. Tropics (3 S)	0.22	0.19	0.23	0.24
Atlantic S. Tropics (19 S)	0.13	0.10	0.16	0.16
Atlantic S. Low Lat. (34 S)	0.14	0.10	0.15	0.16
Atlantic S. Mid Lat. (46 S)	0.21 (0.02)	0.17 (0.01)	0.35 (0.01)	0.35 (0.02)
Pacific N. High Lat. (51 N)	0	0.02	0	-0.02
Pacific N. Mid Lat. (16 N)	0.24	0.25	0.29	0.24
Pacific N. Tropics (3 S)	-0.05	-0.05	-0.04	-0.05
Pacific S. Tropics (19 S)	-0.31	-0.33	-0.28	-0.30
Pacific S. Mid Lat. (46 S)	0.19	0.22	0.30	0.19
Indian Tropics (19 S)	-0.11	-0.11	-0.15	-0.10
Indian S. Mid Lat. (42 S)	0.14	0.15	0.32	0.18

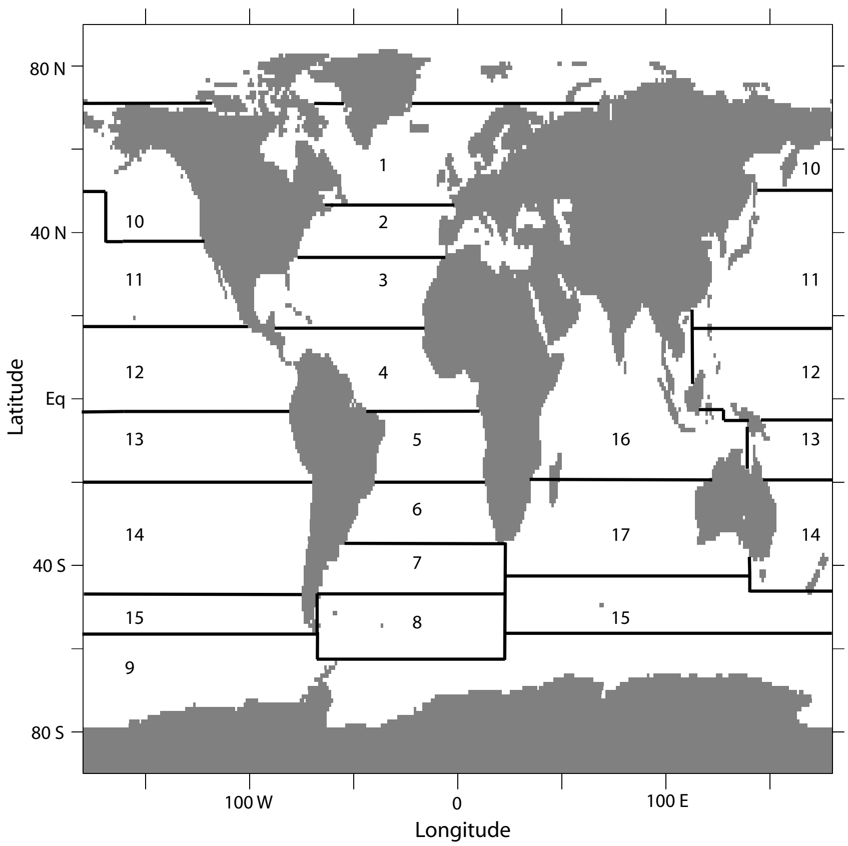

Figure 1. Supplement material Figure S1: Map of the 17 regions used in the EnKF inversion.

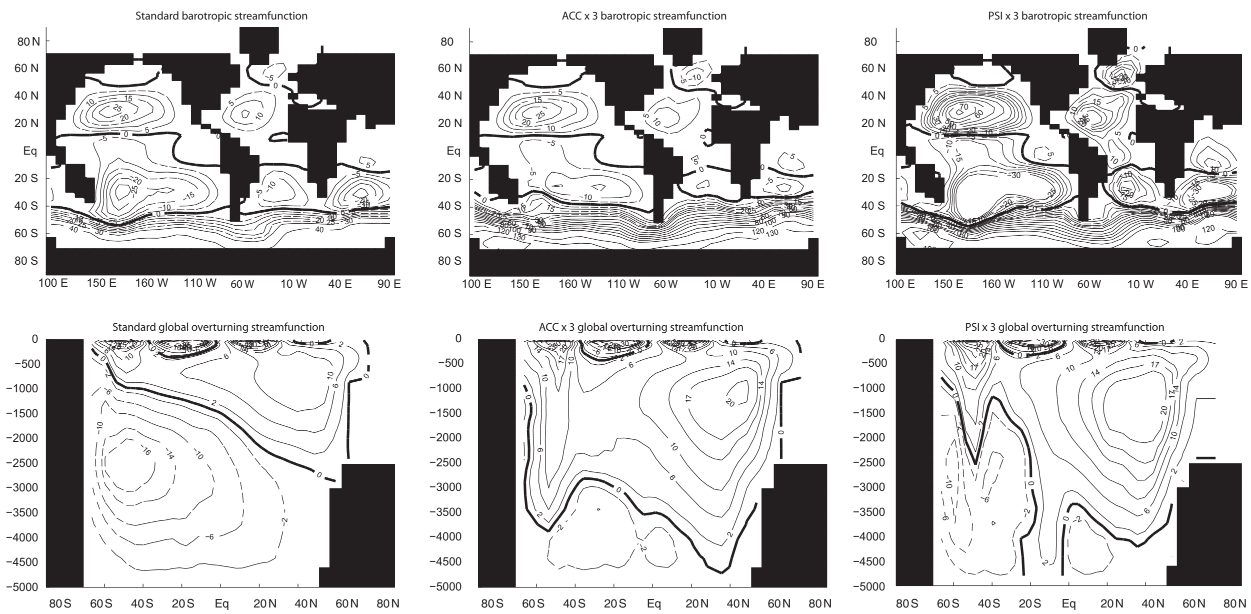

Figure 2. Supplement material Figure S2: Global streamfunction and Global Overturning for the Standard, ACC × 3 and PSI × 3 Bern3D model setup.

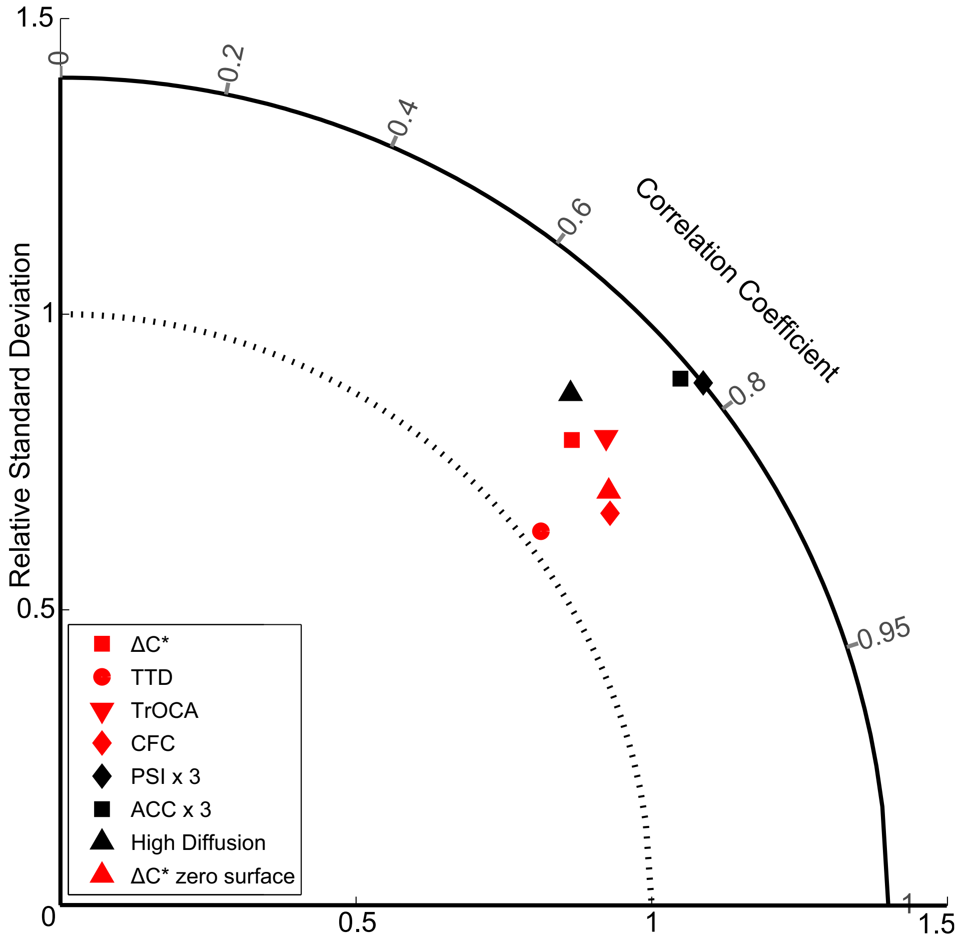

Figure 3. Supplement material Figure S3: Taylor diagram for the different Bern3D model setups and the different data-based reconstructions compared with the pCO_2 based estimates of *Takahashi et al* [2008]. The red symbols are the different data-based simulations, the black ones represent the different Bern3D model setups.